



Exploring Three-Dimensional MHD Maxwell Hybrid Nanofluid Flow: A Computational Study on a Stretching sheet

Hamzeh T. Alkawasbeh*

Department of Mathematics, Faculty of Science, Ajloun National University, P.O. Box 43, Ajloun 26810, Jordan

Abstract

Hybrid nanofluid's applications are diverse and encompass fields such as chemical engineering, microelectronics, solar energy, cooling systems, electronics, and power-saving technologies, where their enhanced heat transfer properties offer significant advantages. In this study, a three-dimensional Maxwell hybrid nanofluid under MHD effects is analyzed and shown across a stretched sheet. Molybdenum disulfide (MoS_2) and graphene oxide (GO) nanoparticles combined with ethylene glycol (EG) make up the hybrid nanofluid. Coupled nonlinear partial differential equations are used to describe the controlling equations. These equations are then converted into coupled nonlinear ordinary differential equations using similarity transformations. Through the use of MATLAB programming and the *bvp4c* technique, these equations may be solved numerically. Figures and tables that illustrate the effects of the Deborah number, magnetic parameter, rotational parameter, and volume percentage of nanoparticles on temperature, velocity, skin friction coefficient, and Nusselt number have been studied. The salient characteristics are: The velocity decreases with increasing Deborah number, magnetic parameter, and rotational parameter values. The findings indicate that the surface temperature is increased by higher values of the Deborah number, magnetic parameter, and rotational parameter. The hybrid nanofluid exhibits greater values of temperature, velocity, and Nusselt number in comparison to the nanofluid. A comparison analysis agrees well with the previous studies.

Keywords: Stretching Sheet; Magnetohydrodynamics MHD; Maxwell fluid; Hybrid nanofluid.

1 Introduction

Nanotechnology finds diverse applications in various manufacturing processes, such as solar energy systems [1], inkjet printers [2], geothermal systems [3, 4], electrical gadgets, biomedical devices [4], and the cooling of metallic plates [5]. Nanofluids (NFs) represent blends of liquid and solid nanomaterials with dimensions around 100 nm. These mixtures demonstrate exceptionally elevated thermal conductivity and thermal diffusivity, paving the way for innovative and superior solutions in thermal applications.

* Corresponding author. Tel.: +962798662512

E-mail address: alkawasbeh@gmail.com, & alkawasbeh@anu.edu.jo

In the pursuit of enhancing nanofluid properties, a recent advancement involves the development of hybrid nanofluids (HBNFs), representing an evolved category of nanofluids. These HBNFs consist of diverse types of nanoparticles either blended together or in compound form. A fundamental principle underlying HBNFs is the dispersion of two distinct types of nanomolecules within the base liquid. This, in comparison to conventional nanofluids, elevates the heat exponent of typical fluids, thereby augmenting their heat transmission capabilities. Anuar et al. [6] investigated the hybrid flow characteristics of a contracted/expanded Ag-MgO/water nanofluid over an inclined surface. They concluded that skin friction and the local Nusselt number are significantly increased by an increase in tilt angle. Hamid et al. [7] on the heat transfer capacities of TiO₂-SiO₂/water hybrid NF found that the greatest improvement in heat transmission rate was 22.1%, which corresponds to a volume fraction of 3.0% for nanoparticles. Eid et al. [8] found that the hybrid nanofluid's rate of heat transfer in a shrinkable container increases with the concentration of Fe₃O₄/EG nanoparticles in their study of the magnetic Fe₃O₄-Cu/EG hybrid nanofluid flow. Ashorynejad [9] investigated how a hybrid nanofluid inside of an open cavity may improve thermal efficiency. They found that when the volume fraction of the nanoparticles increases, heat transfer increases. An inclined magnetic force was applied while researching the Oldroyd B hybrid nanofluid by Nayak et al. [10]. Their findings indicate that when the inclination angle of the applied magnetic field increases, the velocity profile decreases. Heat and mass transfer rates rose when CNTs and Fe₃O₄/water nanoparticles were mixed with water, according to Tassaddiq et al. [11]. Their analysis of the heat and mass transfer of a hybrid nanofluid flow consisting of CNT-Fe₃O₄ and water, produced by a revolving disc, served as the foundation for this. It has been established that Lorentz force is responsible for the temperature of the hybrid nanofluid to rise when MHD is present in the flow of the hybrid nanofluid across a thin cylinder, which Patil et al. [12] by studied the effect of MHD on mixed convective hybrid nanofluid. According to Lund et al. [13], in their study of the MHD flow of Al₂O₃-Cu hybrid nanofluid over a nonlinear shrinking sheet, they discovered that the hybrid nanofluid had a greater rate of heat transfer than either a simple nanofluid or viscous fluid.

Comprehending the dynamics of non-Newtonian fluid motions is essential for numerous industrial and technological applications, such as manufacturing glass fibers, producing plastic films, crystal growth, and paper production. Alkasasbeh and Mohamed [14] presented a flow and heat transfer study using Williamson model on MHD (SWCNTS+MWCNTS)/H₂O-Based hybrid nanofluids over exponentially shrinking sheets. Bouselsal et al. [15] provided insights into the heat transfer enhancement using Al₂O₃-MWCNT/water hybrid nanofluid in a tube/shell heat exchanger, with a focus on the impact of different tube shapes and flow velocities. The presence of non-Newtonian fluids in various industrial and technical processes has spurred extensive research efforts, leading researchers to explore and analyze their utility across a broad spectrum of chemical, biological, and other processes [16], [17]. Currently, there is no comprehensive equation model capable of fully capturing all features of non-Newtonian fluid flow. Non-Newtonian fluids are widely classified as differential, integral, or rate-type fluids, prompting researchers to develop constitutive equations based on this categorization to evaluate their behaviour in a variety of natural events. Some scientists choose to combine the Cattaneo-Christov model with other fluid models, such as the Jeffrey fluid model [18], the Williamson model [19], the Prandtl fluid model, and the Eyring-Powell model [20].

Several investigations on non-Newtonian nanofluids have focused on various geometrical and material properties, notably using the Maxwell model. The rate-type Maxwell fluid serves as an efficient tool for displaying relaxation time features. Lubricants, polymer solutions, and crude oil are examples of Maxwell fluids. Extensive research has been conducted on non-Newtonian fluids under various geometrical and material conditions. In the case of an upper convected Maxwell fluid (UCM), Abel et al. [21] delved into the impacts of (MHD) flow and heat transfer over a deformable sheet. They observed that an increase in the magnetic parameter led to a reduction in velocity, attributed to the Lorentz force a drag-like force arising from the magnetic field that opposes the momentum of fluid particles. Prasannakumara et al. [22] investigated a Maxwell nanofluid's (MHD) boundary layer mixed convective flow. Their research concentrated on the flow of a nanofluid across a bidirectionally expanding surface in the presence of nonlinear radiation. The findings show that nonlinear thermal radiation has a bigger impact on the temperature field than linear thermal radiation. Safdar et al. [23] have investigated the MHD effects in a convective-heated Maxwell nanofluid flow across a porous stretched sheet containing gyrotactic microorganisms. Their findings revealed that when the bio-convection parameter and Peclet number increase in size, so does the microorganism field.. Shah et al. [24] analyzed the flow of an Upper Convected Maxwell (UCM) nanofluid generated by an inclined stretching sheet through porous media and under the influence of a magnetic field, considering slip and radiative effects. Meanwhile, Khan et al. [25] investigated the impact of thermal and solutal stratifications on the flow of a Maxwell fluid with varying thicknesses. Their results indicated an increase in the velocity profile with higher values of viscosity and Maxwell fluid factors, while the concentration and temperature profiles decreased with the solutal stratification parameter. Additionally, Biswas et al. [26] studied the (MHD) flow behavior of a two-dimensional Maxwell nanofluid over a stretched sheet to simulate Brownian motion. Their findings highlighted that both heat source and radiation parameters contribute to adequate heat in the fluid, suggesting that the addition of radiation factors thickens the thermal boundary layer. Ahmad et al. [27] investigated the effects of a heat source/sink on the stagnation point flow of a Maxwell nanofluid across a

permeable spinning disc. Their studies demonstrated that when the thermophoresis factor increases, the heat transfer rate decreases, and rotation accelerates heat transfer at the disc surface. As detailed in references [28-38], several further studies on Maxwell nanofluid flow have been conducted over a variety of geometries, including parallel plates, bidirectional stretching sheets, wedges, and parallel discs.

The main objective of this article is to provide an analytical investigation of the magnetohydrodynamics (MHD) of a Maxwell hybrid nanofluid over a stretching surface. The study delves into the effects of the Deborah number, magnetic parameter, rotational parameter, and volume fraction of nanoparticles on both the flow pattern and heat transfer rate, presenting and discussing their influences. The analytical solution for the governing equations of the system is obtained using the bvp4c method, implemented in MATLAB.

2. Mathematical Analysis

An incompressible, rotating, laminar, and three-dimensional Maxwell hybrid nanofluids stream is described over a linearly stretching sheet. The hybrid nanofluids contain fluids such as ethylene glycol (EG) as the base fluid and two solid nanoparticles of molybdenum disulfide (MoS₂), and Graphene oxide GO. As depicted in Figure 1, the sheet contacts the plane at $z = 0$, and fluid motion is kept at $z > 0$. The surface is expanded along the x -axis with a velocity of $u_w(x)$ equal to the distance from the origin to the stretching point. As well, the fluid spins continuously around the z -axis with a constant angular velocity $\bar{\Omega}$, where $\Omega = [0, 0, \bar{\Omega}]$. Throughout the system, the z -direction is oriented transverse to the plane of the sheet (x, y -plane). In order to consider the MHD effect, a uniform magnetic field (B_0) is applied to the surface normally. T_w is the stretching surface temperature that stays stable, and ($T_w > T_\infty$) where T_∞ is the ambient temperature. In the current flow situation, the velocity vector is $\Lambda = [u_1(x, y, z), u_2(x, y, z), u_3(x, y, z)]$

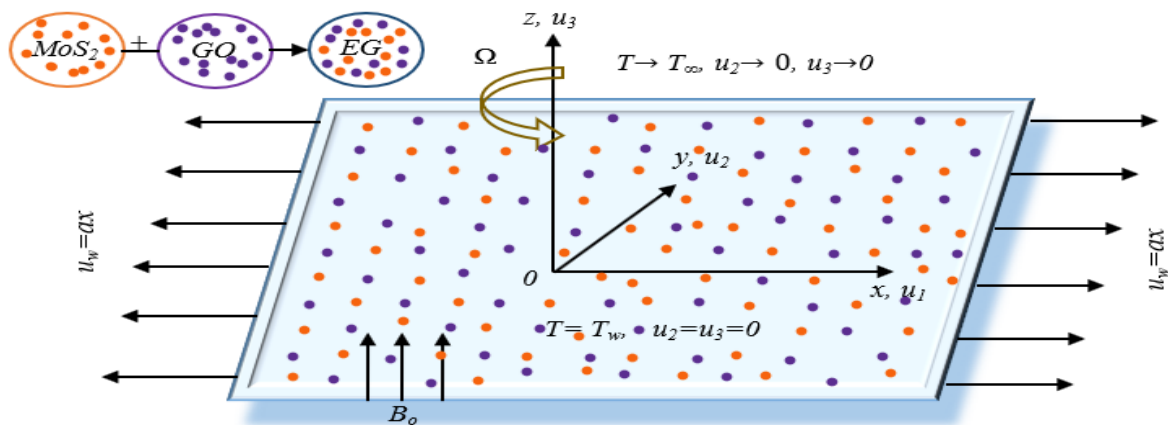


Fig 1: Physical configuration and coordinate system.

The equations for mass, momentum and energy conservation read: [39, 40]:

$$\frac{\partial u_1}{\partial x} + \frac{\partial u_2}{\partial y} + \frac{\partial u_3}{\partial z} = 0, \tag{1}$$

$$u_1 \frac{\partial u_1}{\partial x} + u_2 \frac{\partial u_1}{\partial y} + u_3 \frac{\partial u_1}{\partial z} = 2\bar{\Omega}u_2 + \frac{\mu_{hnf}}{\rho_{hnf}} \left(\frac{\partial^2 u_1}{\partial x^2} + \frac{\partial^2 u_1}{\partial y^2} + \frac{\partial^2 u_1}{\partial z^2} \right) - \frac{\sigma_{hnf}}{\rho_{hnf}} B_0^2 u_1 - \gamma_1 \left\{ \begin{aligned} &u_1^2 \frac{\partial^2 u_1}{\partial x^2} + u_2^2 \frac{\partial^2 u_1}{\partial y^2} + u_3^2 \frac{\partial^2 u_1}{\partial z^2} \\ &+ 2u_1 u_2 \frac{\partial^2 u_1}{\partial x \partial y} + 2u_1 u_3 \frac{\partial^2 u_1}{\partial x \partial z} + 2u_2 u_3 \frac{\partial^2 u_1}{\partial y \partial z} \\ &- 2\bar{\Omega} \left(u_1 \frac{\partial u_2}{\partial x} + u_2 \frac{\partial u_2}{\partial y} + u_3 \frac{\partial u_2}{\partial z} \right) + 2\bar{\Omega} \left(u_2 \frac{\partial u_1}{\partial x} - u_1 \frac{\partial u_1}{\partial y} \right) \end{aligned} \right\}, \tag{2}$$

$$u_1 \frac{\partial u_2}{\partial x} + u_2 \frac{\partial u_2}{\partial y} + u_3 \frac{\partial u_2}{\partial z} = -2\bar{\Omega}u_1 + \frac{\mu_{hnf}}{\rho_{hnf}} \left(\frac{\partial^2 u_2}{\partial x^2} + \frac{\partial^2 u_2}{\partial y^2} + \frac{\partial^2 u_2}{\partial z^2} \right) - \frac{\sigma_{hnf}}{\rho_{hnf}} B_0^2 u_1$$

$$-\gamma_1 \left\{ \begin{aligned} &u_1^2 \frac{\partial^2 u_2}{\partial x^2} + u_2^2 \frac{\partial^2 u_2}{\partial y^2} + u_3^2 \frac{\partial^2 u_2}{\partial z^2} \\ &+ 2u_1 u_2 \frac{\partial^2 u_2}{\partial x \partial y} + 2u_1 u_3 \frac{\partial^2 u_2}{\partial x \partial z} + 2u_2 u_3 \frac{\partial^2 u_2}{\partial y \partial z} \\ &- 2\bar{\Omega} \left(u_1 \frac{\partial u_1}{\partial x} + u_2 \frac{\partial u_1}{\partial y} + u_3 \frac{\partial u_1}{\partial z} \right) + 2\bar{\Omega} \left(u_2 \frac{\partial u_2}{\partial x} - u_1 \frac{\partial u_2}{\partial y} \right) \end{aligned} \right\}, \quad (3)$$

$$u_1 \frac{\partial T}{\partial x} + u_2 \frac{\partial T}{\partial y} + u_3 \frac{\partial T}{\partial z} = \frac{k_{hnf}}{(\rho C_p)_{hnf}} \left(\frac{\partial^2 T}{\partial x^2} + \frac{\partial^2 T}{\partial y^2} + \frac{\partial^2 T}{\partial z^2} \right) - \gamma_2 \left\{ \begin{aligned} &u_1^2 \frac{\partial^2 T}{\partial x^2} + u_2^2 \frac{\partial^2 T}{\partial y^2} + u_3^2 \frac{\partial^2 T}{\partial z^2} \\ &+ 2u_1 u_2 \frac{\partial^2 T}{\partial x \partial y} + 2u_1 u_3 \frac{\partial^2 T}{\partial x \partial z} + 2u_2 u_3 \frac{\partial^2 T}{\partial y \partial z} \\ &+ \left(u_1 \frac{\partial u_1}{\partial x} + u_2 \frac{\partial u_1}{\partial y} + u_3 \frac{\partial u_1}{\partial z} \right) \frac{\partial T}{\partial x} + \left(u_1 \frac{\partial u_3}{\partial x} + u_2 \frac{\partial u_3}{\partial y} + u_3 \frac{\partial u_3}{\partial z} \right) \frac{\partial T}{\partial z} \end{aligned} \right\}. \quad (4)$$

Here, (u_1, u_2, u_3) are the (x, y, z) velocity vectors, B_o denotes the magnetic force, γ_1, γ_2 are the fluid and thermal relaxation time, respectively. T is the fluid's temperature, $(\rho_{hnf}), (\mu_{hnf}), (\sigma_{hnf}), (k_{hnf}), (\rho c_p)_{hnf}$ are the density, dynamic viscosity, electrical conductivity, thermal conductivity and heat capacity of hybrid nanofluid, respectively.

The boundary conditions of the above-explained fluid mathematical model are as follows: [39]:

$$\begin{aligned} u_1 = u_w = ax, u_2 = 0, u_3 = 0, T = T_w \text{ as } z = 0 \\ u_1 \rightarrow 0, u_2 \rightarrow 0, T \rightarrow T_\infty, \text{ as } z \rightarrow \infty. \end{aligned} \quad (5)$$

The hybrid nanofluid thermophysical quantities are expressed as. [14, 41, 42]:

$$\begin{aligned} \rho_{hnf} &= (1 - \chi_{MoS_2})[(1 - \chi_{GO})\rho_{EG} + \chi_{MoS_2}\rho_{MoS_2}] + \chi_{GO}\rho_{GO}, \\ \mu_{hnf} &= \frac{\mu_{EG}}{(1 - \chi_{MoS_2})^{2.5}(1 - \chi_{GO})^{2.5}}, \\ (\rho c_p)_{hnf} &= (1 - \chi_{GO})[(1 - \chi_{MoS_2})(\rho c_p)_f + \chi_{MoS_2}(\rho c_p)_{MoS_2}] + \chi_{GO}(\rho c_p)_{GO}, \\ \frac{k_{hnf}}{k_{bf}} &= \frac{(k_{GO} + 2k_{bf}) - 2\chi_{GO}(k_{bf} - k_{GO})}{(k_{GO} + 2k_{bf}) + \chi_{GO}(k_{bf} - k_{GO})}, \\ \text{where } \frac{k_{bf}}{k_{EG}} &= \frac{(k_{MoS_2} + 2k_f) - 2\chi_{MoS_2}(k_f - k_{MoS_2})}{(k_{MoS_2} + 2k_f) + \chi_{MoS_2}(k_f - k_{MoS_2})}, \\ \alpha_{hff} &= \frac{k_{hnf}}{(\rho c_p)_{hnf}}, \\ \frac{\sigma_{hnf}}{\sigma_f} &= 1 + \frac{3 \left[\frac{\chi_{MoS_2} \sigma_{MoS_2} + \chi_{GO} \sigma_{GO}}{\sigma_f} - (\chi_{MoS_2} + \chi_{GO}) \right]}{\left[\frac{\chi_{MoS_2} \sigma_{MoS_2} + \chi_{GO} \sigma_{GO}}{\sigma_f} + 2 \right] - \left[\frac{\chi_{MoS_2} \sigma_{MoS_2} + \chi_{GO} \sigma_{GO}}{\sigma_f} - (\chi_{MoS_2} + \chi_{GO}) \right]} \end{aligned} \quad (6)$$

where χ_{MoS_2}, χ_{GO} are nanoparticles volume fractions for MoS_2 and GO

To simplify the analysis, we apply the following similarity transformation [39]:

$$u_1 = axF'(\eta), u_2 = axH(\eta), u_3 = -\sqrt{av_f}F(\eta), \theta(\eta) = \frac{T - T_\infty}{T_w - T_\infty}, \eta = z \sqrt{\frac{a}{v_f}} \quad (7)$$

Here $\eta, F'(\eta), H(\eta), \theta(\eta)$ are the dimensionless form of the constraint, velocity profile, angular velocity and temperature profile.

By utilizing (7), eq. (1) is instantly satisfied, and eqs. (2) through (5) using eqs. (6) and (7) are written as

$$\frac{K_1}{K_2} F''' + 2\lambda(H - \beta FH') + \beta(-F'''F^2 + 2F'FF'') + FF'' - (F')^2 - \frac{K_3}{K_2} MF' = 0 \quad (8)$$

$$\frac{K_1}{K_2} H'' + FH' - F'H - 2\lambda[\beta(F'^2 - F''F + H^2) + F'^2] + \beta(-H''F^2 + 2H'F'F) - \frac{K_3}{K_2} MH = 0 \quad (9)$$

$$K_4(1 + \omega\theta)\theta'' + \omega\theta'^2 + Pr F \theta' - Pr \gamma (FF'\theta' + F^2\theta'') = 0 \quad (10)$$

Boundary conditions:

$$\begin{aligned} F = H = 0, F' = 1, \theta = 1, \text{ at } \eta = 0, \\ F' \rightarrow 0, H \rightarrow 0, \theta \rightarrow 0, \text{ as } \eta \rightarrow \infty \end{aligned} \quad (11)$$

where

$$\begin{aligned} K_1 &= \frac{1}{(1-\chi_{MoS_2})^{2.5}(1-\chi_{GO})^{2.5}}, \\ K_2 &= (1-\chi_{MoS_2})[(1-\chi_{GO})\rho_{EG} + \chi_{MoS_2}\rho_{MoS_2}] + \chi_{GO}\rho_{GO} \\ K_3 &= 1 + \frac{3 \left[\frac{\chi_{MoS_2}\sigma_{MoS_2} + \chi_{GO}\sigma_{GO}}{\sigma_f} - (\chi_{MoS_2} + \chi_{GO}) \right]}{\left[\frac{\chi_{MoS_2}\sigma_{MoS_2} + \chi_{GO}\sigma_{GO}}{\sigma_f} + 2 \right] - \left[\frac{\chi_{MoS_2}\sigma_{MoS_2} + \chi_{GO}\sigma_{GO}}{\sigma_f} - (\chi_{MoS_2} + \chi_{GO}) \right]} \\ K_4 &= \frac{\frac{k_{hnf}}{k_{bf}}}{(1-\chi_2) \left[(1-\chi_{MoS_2})(\rho c_p)_{EG} + \chi_{MoS_2} \frac{(\rho c_p)_{MoS_2}}{(\rho c_p)_{EG}} \right] + \frac{\chi_{GO}(\rho c_p)_{GO}}{(\rho c_p)_{EG}}} \end{aligned}$$

The non-dimensional factors are β, M, λ and Pr which represent the Deborah number, magnetic factor, rotational factor and Prandtl number, respectively.

$$\beta = a\gamma_1, M = \left(\frac{\sigma_f B_0^2}{\rho \nu} \right), Pr = \frac{\nu_f (\rho c_p)_f}{k_f}, \lambda = \frac{\bar{n}}{a}, k_f = k_\infty \left(1 + \omega \frac{T - T_\infty}{T_w - T_\infty} \right) \quad (13)$$

in which $\omega > 0$ is a positive constant and k_∞ denotes the thermal conductivity at the ambient.

The skin friction coefficient C_f and Nusselt number Nu , which are important in this problem, can be expressions as [39, 40]:

$$Cf_x = \frac{\bar{\tau}_{xz}}{\rho_{hnf} U_w^2}, Cf_y = \frac{\bar{\tau}_{yz}}{\rho_{hnf} U_w^2}, Nu_x = \frac{x \bar{q}_w}{k_{EG}(T_w - T_\infty)} q_w, \quad (14)$$

where

$$\bar{\tau}_{xz} = \mu_{hnf} \left(\frac{\partial u_3}{\partial x} + \frac{\partial u_1}{\partial z} \right)_{z=0}, \bar{\tau}_{yz} = \mu_{hnf} \left(\frac{\partial u_3}{\partial y} + \frac{\partial u_2}{\partial z} \right)_{z=0}, \bar{q}_w = -k_{hnf} \left(\frac{\partial T}{\partial z} \right)_{z=0}. \quad (15)$$

Using the transformations described above then the (Cf_x, Cf_y) along with the x -axis, y -axis respectively, and Nu written as

$$\sqrt{Re_x} Cf_x = \frac{K_1}{K_2} F''(0), \sqrt{Re_x} Cf_y = \frac{K_1}{K_2} H'(0), \frac{Nu}{\sqrt{Re_x}} = -\frac{k_{hnf}}{k_f} \theta'(0). \quad (16)$$

Where

$$\sqrt{Re_x} = x \sqrt{\frac{a}{\nu_{EG}}} \text{ is the local Reynolds number.}$$

3- Numerical Procedure

We obtained numerical results for MoS_2 -GO/EG and MoS_2 /EG with MATLAB's `bvp4c` function. The findings of the research are presented in a graphical and tabular format, with the emphasis being placed on the mathematical components of the model and the impact that they have on velocity, temperature, and other physical interest factors. To use this approach, first, the ODEs are converted into the system of 1st order differential equations, which is followed as,

$$\begin{cases} y_1 = F, y_2 = F', y_3 = F'', yy_a = F''' \\ y_4 = H, y_5 = H', yy_b = H'' \\ y_6 = \theta, y_7 = \theta', yy_c = \theta'' \end{cases} \quad (17)$$

$$yy_a = \left[\frac{1}{\left(\frac{K_1}{K_2} - \beta y_1^2 \right)} \right] \left[-2\lambda(y_4 - \beta y_1 y_5) - 2y_1 y_2 y_3 - y_1 y_3 + y_2^2 + \left(\frac{K_3}{K_2} \right) M y_2 \right] \quad (18)$$

$$yy_b = \left[\frac{1}{\left(\frac{K_1}{K_2} - \beta y_1^2\right)} \right] \left[y_1 y_5 - y_2 y_4 + 2\lambda[\beta(y_2^2 - y_1 y_3 + y_4^2) + y_2^2] \right] \quad (19)$$

$$yy_c = \left[\frac{1}{(K_4(1+\omega y_6) + y_1^2)} \right] [\omega y_7^2 - Pr(y_1 y_7 + \gamma y_1 y_2 y_7)] \quad (20)$$

Corresponding boundary conditions are converted as:

$$\begin{cases} y_1(0) \\ y_2(0) - 1 \\ y_2(\infty) \\ y_4(0) \\ y_4(\infty) \\ y_6(0) - 1 \\ y_6(\infty) \end{cases} \quad (21)$$

The numerical simulations for different physical phenomena parameters were carried out for the proper computational domain $[0,6]$ rather than $[0,\infty]$, where was fixed at 6 since there is no more variance in the findings at $\eta = 6$. The iterative process's stopping criteria were 10^{-4} . In comparison to other boundary value problem solvers, bvp4c is an excellent solver for a system of ODEs. It's simple to set up in MATLAB and has a cheap processing cost.

4- Results and Discussion

The influence of the most important parameters on the heat transfer rate, fluid friction, velocity and temperature profile is presented in this section. Indeed, the effect of fluid relaxation time on fluid and thermal flow are characterized by the Deborah number $\beta = 0.3, 0.9, 1.5$. In addition, the influence of the magnetic field is presented, varying the magnetic parameter $M = 2, 6, 10$. In another hand, the Angular velocity of the fluid spins has been varied using the rotational parameter $\lambda = 1, 2, 3$.

Table 1. Thermo-physical characteristics of methanol and metals nanoparticles [39, 40]

	$\rho(kgm^{-3})$	$C_p(Jkg^{-1}K^{-1})$	$k(Wm^{-1}K^{-1})$	$\sigma(Sm^{-1})$
EG	1113.5	2430	0.253	4.3×10^{-5}
MoS ₂	5060	397.21	904.21	2.09×10^{-5}
GO	1800	717	5000	1.1×10^{-5}

In the first part of this work, we have explored the influence of fluid relaxation time characterized by the parameter β on the velocity profile of the nanofluid (see Fig.2). Indeed, Fig.2 displays the variation of velocity along to η axis. In this figure, we have deduced that the velocity of the nanofluid with GO+MoS₂/EG is more important than the velocity of the nanofluid occupied by MoS₂/EG nanoparticles. This is likely due to the fact that the GO nanoparticles are heavier than MoS₂ nanoparticles. In this case, we can notice that there is an interaction between volume forces due to fluid weight and buoyancy force due to temperature difference. The same remark can be deduced from Fig.3 concerning the comparison between the two types of nanofluid. Concerning the effect of casson parameter β , as depicted in this figure. The increase in the (β) leads to a rise in the fluid viscosity, resulting in resistance to the motion of the fluid. This is supported by the observation that the velocity profile and the boundary layer thickness decrease for higher values of β .

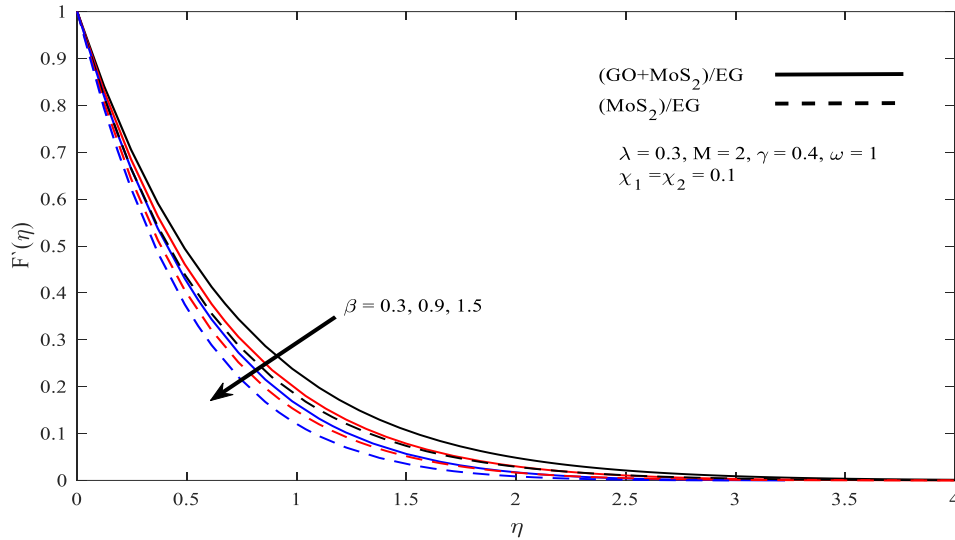


Fig 2: The Velocity Profile with β

In Fig.3, we have explored the impact of the rotational factor on the velocity profile for both types of nanofluid. From this figure, it is noticed that as the angular velocity increase, the velocity of the nanofluid decrease. The impact of the magnetic field on the velocity profile was explored by varying the magnetic factor M . As depicted in Fig.4, the magnetic field negatively affects the velocity of both types of nanofluid. This is due to the character of the confinement by the magnetic field on the thermal convection. This is due to the interaction of electric and magnetic fields, leading to the generation of the Lorentz force, which acts as a resistive force against the fluid motion.

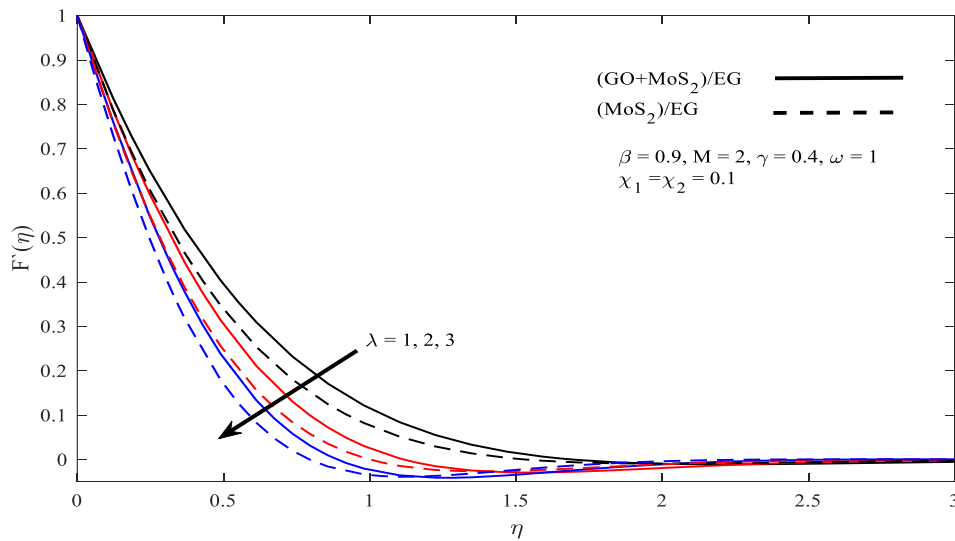


Fig 3: The Velocity Profile with λ

The impacts of the same factors on the angular velocity profile for both types of nanofluid are displayed in Fig.5, 6 and 7. These figures show a decreasing evolution of the angular velocity near the surface, then an increasing evolution away from the surface, and finally, constant values of angular velocity farther from the surface are recorded. From Fig.5, near the surface (near $\eta=0$), the velocity curves of the two types of nanofluid are identical; however, far from the surface, the angular velocity of the MoS_2/EG -based nanofluid is larger than that of the $(\text{GO}+ \text{MoS}_2)/\text{EG}$ based one. Also, it was shown at the sections near the surface that as Deborah number indicates a longer relaxation time, which can lead to a decrease in the fluid's response to stress or strain, including the angular velocity of both types of nanofluid decreases, while at the sections far from the surface, it was found that the β parameter positively affects the angular velocity of the nanofluid, before the velocity curve is identical for all cases, where β will have no influence on the angular velocity for sections farther from the surface.

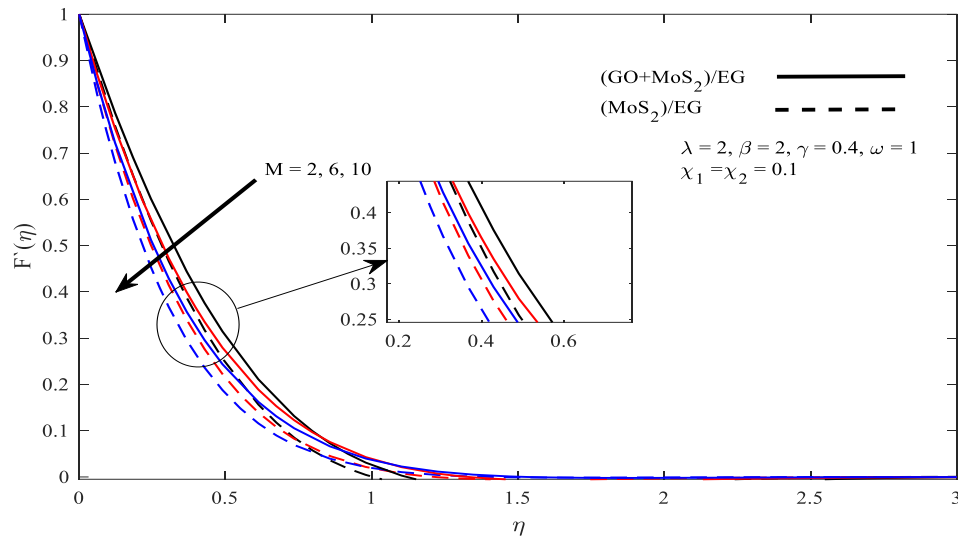


Fig 4: The Velocity Profile with M

The same remarks can be deduced from the two figures 6 and 7, regarding the effects of the rotational factor and the magnetic factor. A descending evolution of the temperature of the nanofluid of different types as a function of the abscissa η (see Fig.8, 9, 10 and 11). In all cases, the temperature of the GO+ MoS₂/EG-based nanofluid is higher than that of the MoS₂/EG-based nanofluid. By increasing the value of the β parameter, the temperature of both types of nanofluid increases (see Fig.8), and when the value of λ , M and ω are augmented, the temperature of nanofluid are increased (see Fig.9, 10 and 11).

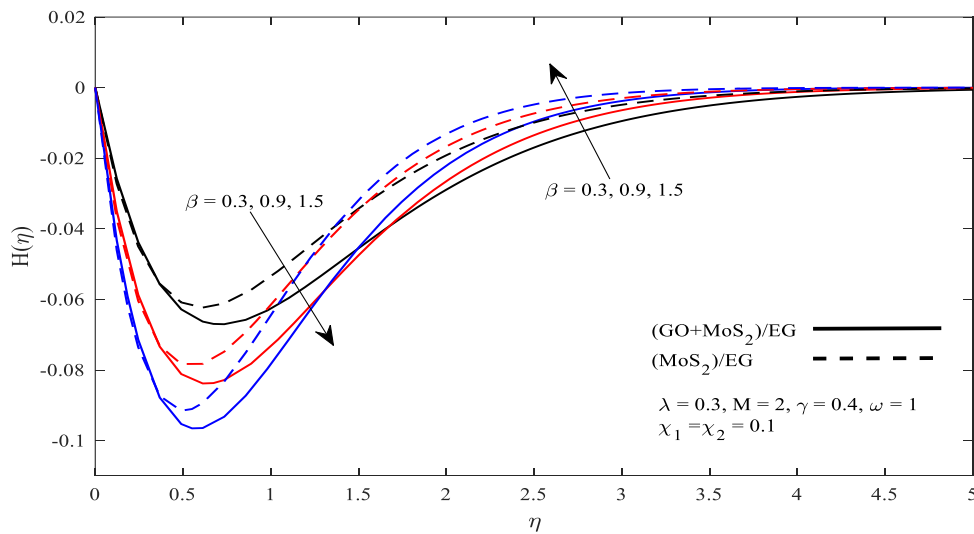


Fig 5: The Angular Velocity Profile with β

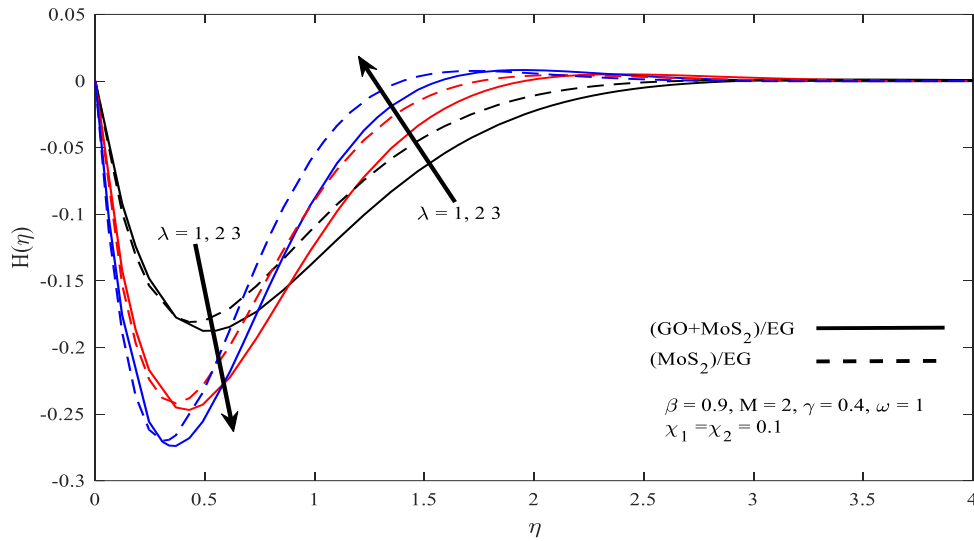


Fig 6: The Angular Velocity Profile with λ

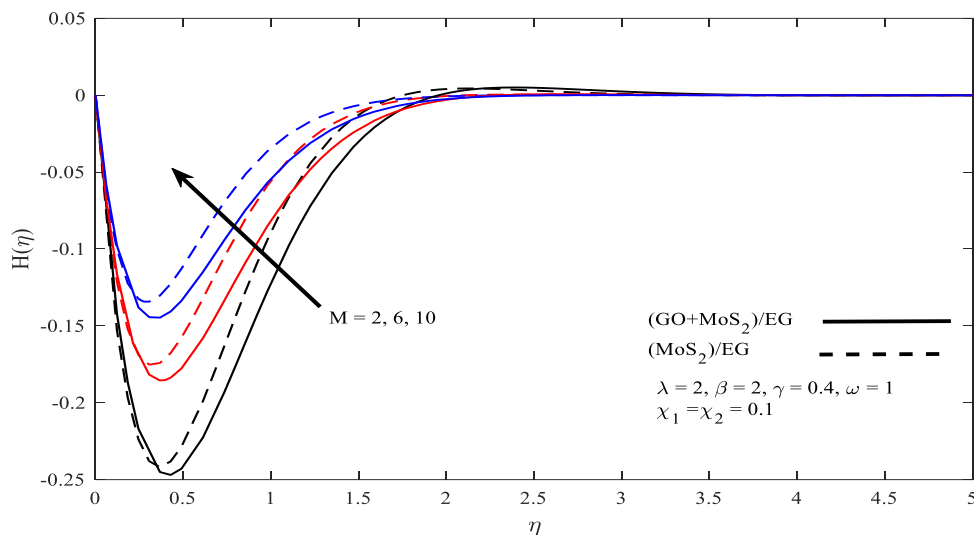


Fig 7: The Angular Velocity Profile with M

To characterize the sliding force versus the maintaining force, we have explored the impact of the previously defined factors on the friction coefficient related to the Reynolds number (see Table.3). As it is indicated in this table, the friction coefficient recorded in a nanofluid based on MoS₂+GO/EG is lower than that of the nanofluid based on MoS₂/EG. As both the M and λ parameters increase, the friction coefficient decreases while increasing β increased fluid friction. To determine the impact of the control parameters on the heat transfer rate in the system, we have explored the effects of the previous parameters on the average Nusselt number related to the Reynolds number. As Table.5 shows, the relative average Nusselt number is more important when using (MoS₂+GO)/EG-based nanofluid compared to the (MoS₂)/EG-based nanofluid. It was also deduced that the heat transfer rate decreases as the λ , β and M parameters increase.

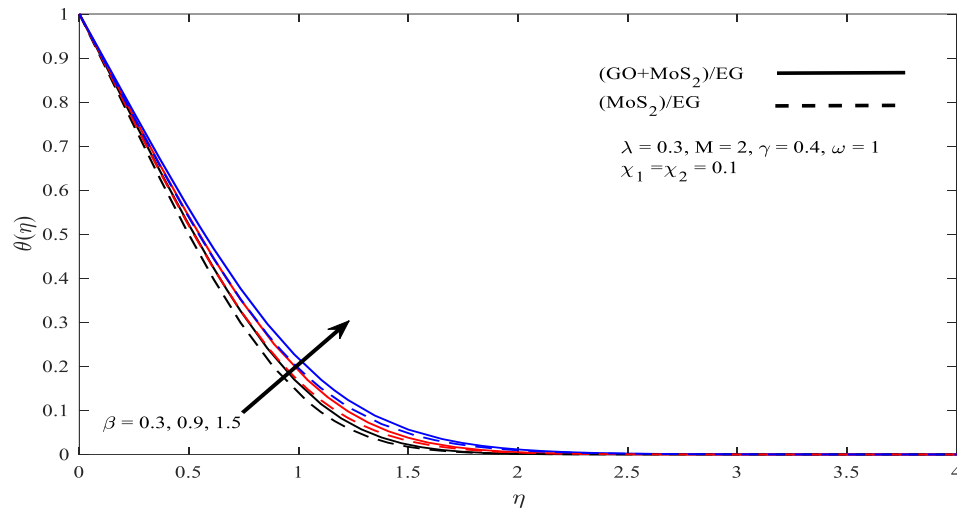


Fig 8: The Temperature Profile with β

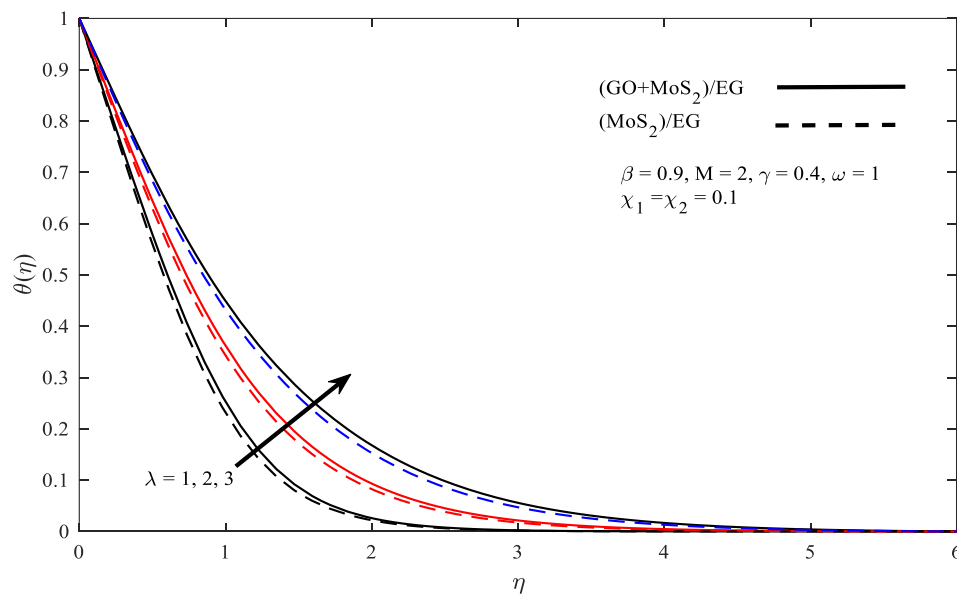


Fig 9: The Temperature Profile with λ

Table 2. Compared value of β on $F''(0)$ and $H'(0)$ when $\lambda = 0.2$ and $\gamma = \omega = M = \chi_{MoS_2} = \chi_{GO} = 0$

β	Mustafa et al. [39]		Present	
	$F''(0)$	$H'(0)$	$F''(0)$	$H'(0)$
0	-1.03312	-0.23856	-1.03310	-0.23854
0.2	-1.08822	-0.28231	-1.08821	-0.28229
0.4	-1.14122	-0.32563	-1.14121	-0.32561
0.6	-1.19231	-0.36873	-1.19230	-0.36870
0.8	-1.21472	-0.41184	-1.21471	-0.41183
1.0	-1.28966	-0.45533	-1.28965	-0.45532
1.2	-1.33635	-0.49968	-1.33634	-0.49967

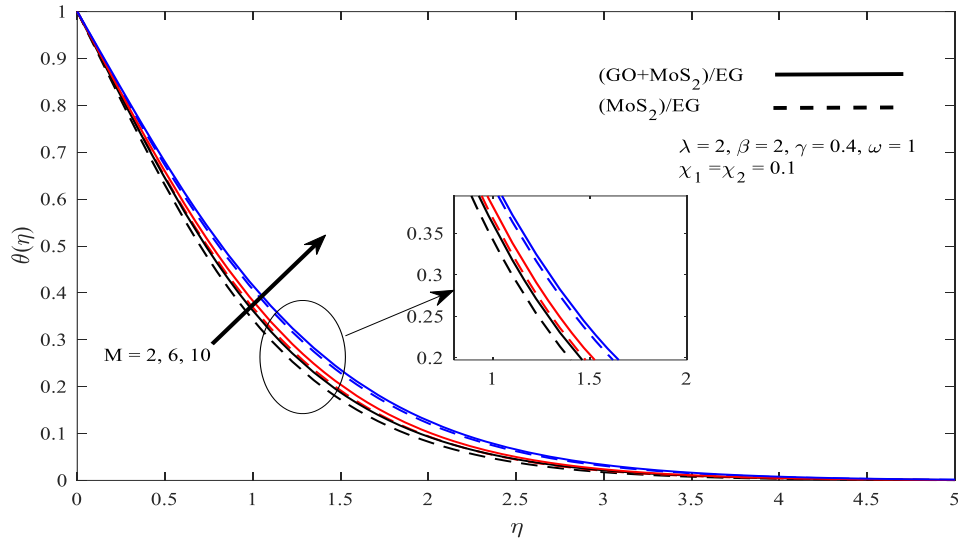


Fig 10: The Temperature Profile with M

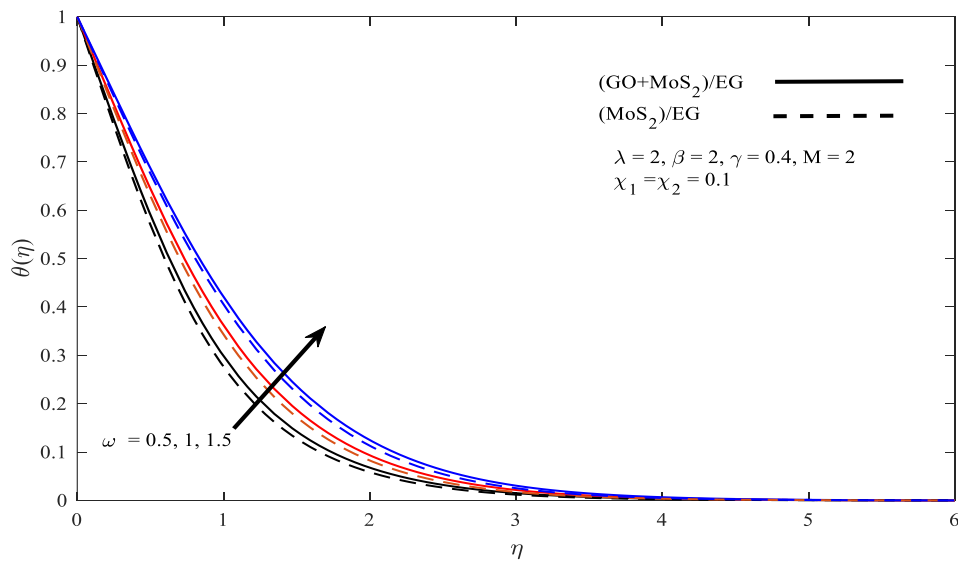


Fig 11: The Temperature Profile with ω

Table 3. Influence of M , β , and λ on $\sqrt{Re_x} Cf_x$

M	β	λ	(MoS ₂ +GO)/EG	(MoS ₂)/EG
2	0.9	2	-2.2689	-2.0376
6			-2.7398	-2.5096
10			-3.1811	-2.9446
2	0.3	2	-2.1393	-1.9243
	0.9		-2.2689	-2.0376
	1.5		-2.3963	-2.1484
2	0.9	1	-1.9952	-1.8037
		2	-2.2689	-2.0376
		3	-2.5308	-2.2646

Table 4. Influence of M , β , and λ on $\sqrt{Re_x}Cf_y$

M	β	λ	(MoS ₂ +GO)/EG	(MoS ₂)/EG
2	0.9	2	-1.8456	-1.6140
6			-1.5747	-1.3528
10			-1.3812	-1.1743
2	0.3	2	-1.4635	-1.2752
	0.9		-1.8456	-1.6140
	1.5		-2.1758	-1.9069
2	0.9	1	-1.1374	-0.9866
		2	-1.8456	-1.6140
		3	-2.3818	-2.0903

Table 5. Impact of M , β , and λ on $\frac{Nu}{\sqrt{Re_x}}$

M	β	λ	(MoS ₂ +GO)/EG	(MoS ₂)/EG
2	0.9	2	2.0224	1.7492
6			1.9423	1.6647
10			1.8281	1.5507
2	0.3	2	2.2026	1.9071
	0.9		2.0224	1.7492
	1.5		1.8433	1.5942
2	0.9	1	2.3816	2.0621
		2	2.0224	1.7492
		3	1.7383	1.5022

5- Conclusion

By taking into account free convection with a constant wall temperature, the current analysis was carried out to study the pattern of flow features and heat transfer in a 3-D maxwell hybrid nanofluid near a stretching sheet at the boundary. Deborah number, magnetic parameter, rotational parameter, the volume fraction of nanoparticles, and Prandtl number were explored for their influencing effects. Using similarity transformations, the PDEs were converted into ODEs. These equations are given a numerical solution in MATLAB using the bvp4c method. The results which were obtained have been compared with published data. The agreement is noted to be excellent.

The significant findings are listen below:

- A drop of velocity is observed and caused by an increase in the Deborah number, magnetic parameter, and rotational parameter.
- An increase in Deborah number when $\eta > 2$ and rotational parameter when $\eta > 1$ has led to an upsurge in the angular velocity profile. Moreover, we obtained the opposite results when $0 \leq \eta \leq 2$ for the Deborah number and also $0 \leq \eta \leq 1$ for the rotational parameter.
- Higher values of the magnetic factor directly caused an increase in the angular velocity profile.
- We discovered that the temperature is rising together with the Deborah number, magnetic parameter, and rotational parameter.
- The velocity, temperature and Nusselt number for the GO+ MoS₂/EG-based nanofluid are higher than that of the MOS₂/EG-based nanofluid, and the opposite happens for angular velocity and Skin friction coefficient along the x -axis and y -axis
- As the Deborah number, magnetic parameter, and rotational parameter increased, the Skin friction coefficient along with the x -axis decreased.
- Nusselt number is shown to be inversely correlated with the values of the Deborah number, magnetic factor, and rotational parameter.

The future research in this context holds potential for expanding the understanding of the behavior of Maxwell hybrid nanofluids under various flow and heat transfer conditions, contributing to the development of more comprehensive models and applications for these nanofluids.

Acknowledgments

The authors would like to thank the Deanship of Scientific Research at Ajloun National University for supporting this work by Grant Code: (11ANU1247).

Nomenclature

B_0	Magnetic Field Strength, (Wb)
Cf	Local Skin Friction Coefficient,
c_p	Specific Heat Capacity, ($Jkg^{-1}K^{-1}$)
H	Angular Velocity ($rad\ s^{-1}$)
k	Thermal Conductivity ($Wm^{-1}K^{-1}$)
M	Magnetic Parameter (Wb)
Nu	Nusselt Number
Pr	Prandtl Number
\bar{q}	Heat Flux, (Wm^{-2})
Re	Local Reynolds Number.
T	Temperature, (K)
T_o	Reference Temperature, (K)
u_w	Variable Shrinking Velocity, (Ms^{-1})
V_w	Variable Velocity of Suction/Injection, (Ms^{-1})
u_1	Velocity Component Along x-axis, (Ms^{-1})
u_2	Velocity Component along y-axis, (Ms^{-1})
u_3	Velocity Component along z-axis, (Ms^{-1})

Greek Symbols

μ	Dynamic Viscosity, ($Kgm^{-1}s^{-1}$)
ν	Kinematic Viscosity, (M^2s^{-1})
ρ	Density, (kgm^{-3})
σ	Electrical Conductivity, ($A^2s^3kg^{-1}m^{-1}$)
$\bar{\Omega}$	Constant Angular Velocity ($rad\ s^{-1}$)
Λ	Velocity Vector
γ_1, γ_2	Fluid and Thermal Relaxation Time
η	Dimensionless Form of The Constraint
θ	Temperature Profile.
β	Deborah Number
λ	Rotational Factor
ω	Positive Constant
$\bar{\Omega}$	Constant Angular Velocity
Λ	Velocity Vector
Ψ	Stream Function, ($Kgm^{-1}s^{-1}$)
$\bar{\tau}$	Wall Shear Stress, ($Kgm^{-1}s^{-2}$)
χ	Nanoparticle Volume Fraction ($molm^{-3}$)

Subscripts

f	Base Fluid
hnf	Hybrid Nanofluid
w	Wall/Surface
∞	Ambient Environment

References

- [1] W. Jamshed, N. A. A. M. Nasir, S. S. P. M. Isa, R. Safdar, F. Shahzad, K. S. Nisar, M. R. Eid, A.-H. Abdel-Aty, I. Yahia, Thermal growth in solar water pump using Prandtl–Eyring hybrid nanofluid: a solar energy application, *Scientific reports*, Vol. 11, No. 1, pp. 18704, 2021.
- [2] A. Kosmala, Q. Zhang, R. Wright, P. Kirby, Development of high concentrated aqueous silver nanofluid and inkjet printing on ceramic substrates, *Materials Chemistry and Physics*, Vol. 132, No. 2-3, pp. 788-795, 2012.
- [3] Z. Liu, X. Yang, H. M. Ali, R. Liu, J. Yan, Multi-objective optimizations and multi-criteria assessments for a nanofluid-aided geothermal PV hybrid system, *Energy Reports*, Vol. 9, pp. 96-113, 2023.
- [4] M. Soltani, F. M. Kashkooli, M. A. Fini, D. Gharapetian, J. Nathwani, M. B. Dusseault, A review of nanotechnology fluid applications in geothermal energy systems, *Renewable and Sustainable Energy Reviews*, Vol. 167, pp. 112729, 2022.

- [5] P. S. Reddy, P. Sreedevi, A. J. Chamkha, Heat and mass transfer flow of a nanofluid over an inclined plate under enhanced boundary conditions with magnetic field and thermal radiation, *Heat Transfer—Asian Research*, Vol. 46, No. 7, pp. 815-839, 2017.
- [6] N. S. Anuar, N. Bachok, I. Pop, Influence of buoyancy force on Ag-MgO/water hybrid nanofluid flow in an inclined permeable stretching/shrinking sheet, *International Communications in Heat and Mass Transfer*, Vol. 123, pp. 105236, 2021.
- [7] K. Hamid, W. Azmi, M. Nabil, R. Mamat, Improved thermal conductivity of TiO₂–SiO₂ hybrid nanofluid in ethylene glycol and water mixture, in *Proceeding of*, IOP Publishing, pp. 012067.
- [8] M. R. Eid, M. A. Nafe, Thermal conductivity variation and heat generation effects on magneto-hybrid nanofluid flow in a porous medium with slip condition, *Waves in Random and Complex Media*, Vol. 32, No. 3, pp. 1103-1127, 2022.
- [9] H. R. Ashorynejad, A. Shahriari, MHD natural convection of hybrid nanofluid in an open wavy cavity, *Results in Physics*, Vol. 9, pp. 440-455, 2018.
- [10] M. K. Nayak, V. S. Pandey, S. Shaw, O. Makinde, K. Ramadan, M. B. Henda, I. Tlili, Thermo-fluidic significance of non Newtonian fluid with hybrid nanostructures, *Case Studies in Thermal Engineering*, Vol. 26, pp. 101092, 2021.
- [11] A. Tassaddiq, S. Khan, M. Bilal, T. Gul, S. Mukhtar, Z. Shah, E. Bonyah, Heat and mass transfer together with hybrid nanofluid flow over a rotating disk, *AIP Advances*, Vol. 10, No. 5, 2020.
- [12] P. Patil, M. Kulkarni, Analysis of MHD mixed convection in a Ag-TiO₂ hybrid nanofluid flow past a slender cylinder, *Chinese Journal of Physics*, Vol. 73, pp. 406-419, 2021.
- [13] L. A. Lund, Z. Omar, I. Khan, E.-S. M. Sherif, Dual branches of MHD three-dimensional rotating flow of hybrid nanofluid on nonlinear shrinking sheet, *Computers, Materials and Continua*, Vol. 66, No. 1, pp. 127-139, 2020.
- [14] H. T. Alkasasbeh, M. K. A. Mohamed, MHD (SWCNTS+ MWCNTS)/H₂O-Based Williamson Hybrid Nanofluids Flow Past Exponential Shrinking Sheet in Porous Medium.
- [15] M. Bouselsal, F. Mebarek-Oudina, N. Biswas, A. A. I. Ismail, Heat Transfer Enhancement Using Al₂O₃-MWCNT Hybrid-Nanofluid inside a Tube/Shell Heat Exchanger with Different Tube Shapes, *Micromachines*, Vol. 14, No. 5, pp. 1072, 2023.
- [16] W.-T. Wu, M. Massoudi, Recent advances in mechanics of non-Newtonian fluids, *Fluids*, Vol. 5, No. 1, pp. 10, 2020.
- [17] F. Selimefendigil, G. Şenol, H. F. Öztop, N. H. Abu-Hamdeh, A Review on Non-Newtonian Nanofluid Applications for Convection in Cavities under Magnetic Field, *Symmetry*, Vol. 15, No. 1, pp. 41, 2022.
- [18] W. Hasona, A. El-Shehkipy, M. Ibrahim, Combined effects of magnetohydrodynamic and temperature dependent viscosity on peristaltic flow of Jeffrey nanofluid through a porous medium: Applications to oil refinement, *International Journal of Heat and Mass Transfer*, Vol. 126, pp. 700-714, 2018.
- [19] P. Sreedevi, P. S. Reddy, Williamson hybrid nanofluid flow over swirling cylinder with Cattaneo–Christov heat flux and gyrotactic microorganism, *Waves in Random and Complex Media*, pp. 1-28, 2021.
- [20] Y.-M. Chu, F. Ahmad, M. I. Khan, M. Nazeer, F. Hussain, N. B. Khan, S. Kadry, L. Mei, Numerical and scale analysis of non-Newtonian fluid (Eyring-Powell) through pseudo-spectral collocation method (PSCM) towards a magnetized stretchable Riga surface, *Alexandria Engineering Journal*, Vol. 60, No. 2, pp. 2127-2137, 2021.
- [21] M. Subhas Abel, J. V. Tawade, M. M. Nandeppanavar, MHD flow and heat transfer for the upper-convected Maxwell fluid over a stretching sheet, *Meccanica*, Vol. 47, pp. 385-393, 2012.
- [22] B. Prasannakumara, M. Gnaneswara Reddy, G. Thamanna, B. Gireesha, MHD Double-diffusive boundary-layer flow of a Maxwell nanofluid over a bidirectional stretching sheet with Soret and Dufour effects in the presence of radiation, *Nonlinear Engineering*, Vol. 7, No. 3, pp. 195-205, 2018.
- [23] R. Safdar, M. Jawad, S. Hussain, M. Imran, A. Akgül, W. Jamshed, Thermal radiative mixed convection flow of MHD Maxwell nanofluid: Implementation of Buongiorno's model, *Chinese Journal of Physics*, Vol. 77, pp. 1465-1478, 2022.
- [24] S. Shah, N. Rafiq, F. A. Abdullah, S. Atif, M. Abbas, Slip and radiative effects on MHD Maxwell nanofluid with non-Fourier and non-Fick laws in a porous medium, *Case Studies in Thermal Engineering*, Vol. 30, pp. 101779, 2022.
- [25] M. Khan, M. Malik, T. Salahuddin, S. Saleem, A. Hussain, Change in viscosity of Maxwell fluid flow due to thermal and solutal stratifications, *Journal of Molecular Liquids*, Vol. 288, pp. 110970, 2019.
- [26] R. Biswas, M. S. Hossain, R. Islam, S. F. Ahmed, S. Mishra, M. Afikuzzaman, Computational treatment of MHD Maxwell nanofluid flow across a stretching sheet considering higher-order chemical reaction and thermal radiation, *Journal of Computational Mathematics and Data Science*, Vol. 4, pp. 100048, 2022.

- [27] J. Ahmed, M. Khan, L. Ahmad, Stagnation point flow of Maxwell nanofluid over a permeable rotating disk with heat source/sink, *Journal of Molecular Liquids*, Vol. 287, pp. 110853, 2019.
- [28] M. Farooq, S. Ahmad, M. Javed, A. Anjum, Magnetohydrodynamic flow of squeezed Maxwell nanofluid with double stratification and convective conditions, *Advances in Mechanical Engineering*, Vol. 10, No. 9, pp. 1687814018801140, 2018.
- [29] P. Sreedevi, P. Sudarsana Reddy, M. Sheremet, Impact of homogeneous–heterogeneous reactions on heat and mass transfer flow of Au–Eg and Ag–Eg Maxwell nanofluid past a horizontal stretched cylinder, *Journal of Thermal Analysis and Calorimetry*, Vol. 141, pp. 533-546, 2020.
- [30] P. Sreedevi, P. S. Reddy, Effect of magnetic field and thermal radiation on natural convection in a square cavity filled with TiO₂ nanoparticles using Tiwari–Das nanofluid model, *Alexandria Engineering Journal*, Vol. 61, No. 2, pp. 1529-1541, 2022.
- [31] S. Manjunatha, B. A. Kuttan, S. Jayanthi, A. Chamkha, B. Gireesha, Heat transfer enhancement in the boundary layer flow of hybrid nanofluids due to variable viscosity and natural convection, *Heliyon*, Vol. 5, No. 4, 2019.
- [32] P. Sreedevi, P. S. Reddy, K. Suryanarayana Rao, Effect of magnetic field and radiation on heat transfer analysis of nanofluid inside a square cavity filled with silver nanoparticles: Tiwari–Das model, *Waves in Random and Complex Media*, pp. 1-19, 2021.
- [33] P. Sreedevi, P. S. Reddy, Combined influence of Brownian motion and thermophoresis on Maxwell three-dimensional nanofluid flow over stretching sheet with chemical reaction and thermal radiation, *Journal of Porous Media*, Vol. 23, No. 4, 2020.
- [34] T. Fahim, S. Laouedj, A. Abderrahmane, S. Alotaibi, O. Younis, H. M. Ali, Heat transfer enhancement in parabolic through solar receiver: a three-dimensional numerical investigation, *Nanomaterials*, Vol. 12, No. 3, pp. 419, 2022.
- [35] P. S. Reddy, P. Sreedevi, A. J. Chamkha, A. F. Al-Mudhaf, Heat and mass transfer boundary-layer flow over a vertical cone through porous media filled with a Cu–water and Ag–water nanofluid, *Heat Transfer Research*, Vol. 49, No. 2, 2018.
- [36] P. S. Reddy, P. Sreedevi, Buongiorno's model nanofluid natural convection inside a square cavity with thermal radiation, *Chinese Journal of Physics*, Vol. 72, pp. 327-344, 2021.
- [37] P. Sudarsana Reddy, P. Sreedevi, Impact of chemical reaction and double stratification on heat and mass transfer characteristics of nanofluid flow over porous stretching sheet with thermal radiation, *International Journal of Ambient Energy*, Vol. 43, No. 1, pp. 1626-1636, 2022.
- [38] M. Uddin, S. Rasel, Numerical analysis of natural convective heat transport of copper oxide-water nanofluid flow inside a quadrilateral vessel, *Heliyon*, Vol. 5, No. 5, 2019.
- [39] M. Mustafa, T. Hayat, A. Alsaedi, Rotating flow of Maxwell fluid with variable thermal conductivity: an application to non-Fourier heat flux theory, *International Journal of Heat and Mass Transfer*, Vol. 106, pp. 142-148, 2017.
- [40] A. A. Akbar, N. A. Ahammad, A. U. Awan, A. K. Hussein, F. Gamaoun, E. M. Tag-ElDin, B. Ali, Insight into the role of nanoparticles shape factors and diameter on the dynamics of rotating water-based fluid, *Nanomaterials*, Vol. 12, No. 16, pp. 2801, 2022.
- [41] H. Alkassasbeh, Numerical solution of heat transfer flow of casson hybrid nanofluid over vertical stretching sheet with magnetic field effect, *CFD Letters*, Vol. 14, No. 3, pp. 39-52, 2022.
- [42] H. T. Alkassasbeh, Numerical Investigation of MHD Carreau Hybrid Nanofluid Flow over a Stretching Sheet in a Porous Medium with Viscosity Variations and Heat Transport, *Journal of Computational Applied Mechanics*, Vol. 54, No. 3, pp. 410-424, 2023.